Available online at www.sciencedirect.com
SCIENCE DIRECT®
European Journal of Medicinal Chemistry 40 (2005) 1111–1122
EUROPEAN JOURNAL OF MEDICINAL CHEMISTRY
www.elsevier.com/locate/ejmech

Original article

The 2-aminoglucosamide motif improves cellular uptake and photodynamic activity of tetraphenylporphyrin

Benoît Di Stasio [a,b], Céline Frochot [a], Dominique Dumas [c], Pascale Even [a], Jurriaan Zwier [d], Audrey Müller [a], Jacques Didelon [b], François Guillemin [b], Marie-Laure Viriot [a], Muriel Barberi-Heyob [b,*]

[a] *DCPR-GRAPP, UMR 7630 CNRS-INPL, Groupe ENSIC, 1, rue Grandville, 54000 Nancy, France*
[b] *Centre Alexis Vautrin, CRAN-UMR 7039 CNRS-UHP-INPL, Avenue de Bourgogne, Brabois, 54511 Vandœuvre-les-Nancy, France*
[c] *LEMTA, Equipe Mécanique et Ingénierie Cellulaire et Tissulaire-Service Imagerie Cellulaire, UMR 7563 CNRS-INPL-UHP, Faculté de Médecine, BP 184, 54505 Vandœuvre-les-Nancy, France*
[d] *University of Amsterdam, Institute of Molecular Chemistry, Organic Photonic Materials Group, Nieuwe Achtergracht 129, 1018 WS, The Netherlands*

Received 8 December 2004; received in revised form 17 March 2005; accepted 27 April 2005

Available online 15 June 2005

Abstract

Several strategies have been proposed to improve the efficiency of photosensitizers used in photodynamic therapy (PDT). In this context, the synthesis of mono- (**1**) and di-glucosylated (**2**) porphyrins, and mono-glucosylated chlorin (**3**) was performed. HT29 human adenocarcinoma cells were significantly more sensitive to asymmetric and less hydrophobic glucosylated photosensitizers-mediated PDT (**1**, **3**), compared to tetraphenylporphyrin (TPP). The lowest photosensitivity observed for TPP was consistent with the lowest uptake. Moreover, the most pronounced photodynamic activity measured for **3** was in relation with the improvement of cellular uptake, the singlet oxygen quantum yield and the high extinction coefficient value at 650 nm compared to porphyrins. Cellular localization analysis showed that **1** and **3** accumulated mainly inside the endoplasmic reticulum.

Keywords: Photodynamic therapy; Glucosylation; Porphyrin; Chlorin; Targeting; In vitro

1. Introduction

Photodynamic therapy (PDT) is a promising treatment for a variety of oncological, cardiovascular, dermatological, and ophthalmic diseases [1]. PDT is based on the use of photosensitizers, which are preferentially taken up and/or retained by diseased tissues. Upon photo-activation with visible light at the appropriate wavelength, the generation of cytotoxic species, such as reactive singlet oxygen, leads to irreversible destruction of the treated tissues [2]. Normal cells, however, are also able to accumulate photosensitizers and be damaged by them, so that prolonged skin photosensitization, light-sensitivity of the eye and other side effects have proved to be severe limitations of PDT.

The ideal drug delivery system should enable the selective accumulation of the photosensitizer within the diseased tissue and the delivery of therapeutic concentrations of photosensitizer to the target site with little or no uptake by non-target cells. The carrier must also be able to incorporate the photosensitizer without loss or alteration of its activity. In view of the high probability of repetitive dosing schedules, the system must also be biodegradable and have little or no immunogenicity [3]. Another reason for using targeting or

Abbreviations: ATP, adenosine triphosphate; Boc, *tert*-butoxycarbonyl; BSA, bovine serum albumin; $CDCl_3$, chloroform-d; CH_2Cl_2, dichloromethane; DCC, dicyclohexylcarbodiimide; DDQ, 2,3-dichloro 5,6-dicyano-1,4-benzoquinone; $DiOC_6$, 3,3-dihexyloxacarbocyanine iodide; DMAP, 4-dimethylaminopyridine; DMF, dimethyl formamide; DMSO, dimethyl sulfoxide; EDCI, 1-(3-dimethylaminopropyl)-3-ethylcarbodiimide hydrochloride; EDTA, ethylene diamine tetra acetic acid; EtOH, ethanol; HCl, hydrochloric acid; BtOH, 1-hydroxybenzotriazole; I.D., internal diameter; KQ, quenching constant; $L.D._{50}$, light doses yielding 50% growth inhibition; MeOH, methanol; $MgSO_4$, magnesium sulfate; MTT, 3-(4,5-dimethylthiazol-2-yl)-2,5-diphenyltetrazolium bromide; $NaHCO_3$, sodium bicarbonate; NaOH, sodium hydroxide; NHS, *N*-hydroxysuccinimide; NMR, nuclear magnetic resonance spectroscopy; PBS, phosphate buffered saline; P1COOH, 4-carboxyphenylporphyrin; PDT, photodynamic therapy; RP-HPLC, reversed phase high performance liquid chromatography; TFA, trifluoroacetic acid; THF, tetrahydrofuran; TMS, tetramethylsilane; TPP, tetraphenylporphyrin.

* Corresponding author. Tel.: +33 3 83 59 83 06; fax: +33 3 83 44 60 71.
E-mail address: m.barberi@nancy.fnclcc.fr (M. Barberi-Heyob).

0223-5234/$ - see front matter © 2005 Elsevier SAS. All rights reserved.
doi:10.1016/j.ejmech.2005.04.007

carriers is to provide an environment where the photosensitizer can be administered in a monomeric form. Indeed, due to their chemical composition, most of the photosensitizers tend to aggregate in aqueous media as a result of the propensity of the hydrophobic skeleton to avoid contact with water molecules [4]. This state is one of the determining factors, which can hinder the efficacy of the drug in vivo by increasing its bioavailability and limiting its capacity to absorb light [5]. An approach developed by several groups is to modulate the amphiphilicity of the photosensitizer [6]. Structural modifications induced by glycoconjugation of the tetrapyrrole system appear as an effective mean to create the equilibrium between hydrophilicity and hydrophobicity. Moser et al. measured a 50–100-fold higher photocytotoxicity for diglucoamido porphyrinoids compared to non glucosylated analogues [7]. The position of sugar substituent is crucial to photo biological activity [8]. Whether glycoconjugation is obviously a good means to introduce such a balance between hydrophilicity and hydrophobicity [9], the nature of the sugar residues seems to take a significant part in the photosensitizing properties and remains to be elucidated. This should be undertaken in the light of the knowledge of the various lectines occurring at the surface of the cell membrane and their implication in glycoconjugated dyes internalization. Pyropheophorbide 2-deoxyglucosamide was evaluated in a 9L glioma rat model as a new photosensitizer targeting glucose transporters (GLUT). Fluorescence imaging studies demonstrated that this conjugate was trapped in tumor via the GLUT/hexokinase pathway [10]. If *O*- or *S*-glycosylated porphyrins have already been synthesized, no report has appeared concerning aminoglycosamide tetraphenyl of porphyrins and chlorin. In comparison with *O*-glycosylated photosensitizers, CONH– glycosyl bonds should resist endogenous hydrolysis catalyzed by glycosidases [11].

In this context, glycosamide porphyrins and the corresponding chlorin have been synthesized in order to study the influence of structural modifications induced by symmetric or asymmetric glycoconjugation on photophysical properties and photosensitivity. Synthesis of mono- and di-glucosylated porphyrins were performed, **1** and **2**, respectively, and the corresponding mono-glucosylated chlorin **3**. The photoactive compounds have been characterized by photophysical properties (molar extinction coefficient, fluorescence and singlet oxygen quantum yields). Cellular internalization process, cellular localization and photocytotoxic properties of **1**–**3** have been compared to those of tetraphenylporphyrin (TPP) in HT29 human adenocarcinoma cells.

2. Results and discussion

2.1. Synthesis, photophysical and chemical characteristics

2.1.1. Synthesis

The synthesis of novel conjugates **1** and **3** is shown in Scheme 1, the synthesis of **2** in Scheme 2. The synthesis of the *O*-acetylated glucosamine has already been described [12].

Synthesis of **1** was carried out in CH_2Cl_2/DMF by coupling the *O*-acetylated glucosamine with 5-(4-carboxyphenyl)-10,15,20-triphenyl-21,23-porphyrin (**4**), mediated by 1-(3-dimethylaminopropyl)-3-ethylcarbodiimide hydrochloride (EDCI) at 0 °C. The compound was purified by chromatography and the yield of pure product was about 65%. The compound **4** was obtained according to the Little method [13] by condensation of pyrrole (4 eq.) with benzaldehyde (3 eq.) and carboxybenzaldehyde (1 eq.) in propionic acid. After purification by SiO_2 and C18 chromatography the yield was 7%. The 5-(4-carboxyphenyl)-5,10,15-triphenyl-chlorin (**5**) was prepared by the diimide reduction of the corresponding porphyrin (yield: 70%) [14]. EDCI has been also used to couple *O*-acetylated glucosamine to the monocarboxyphenyl chlorin **5** to afford the monoglucosylated chlorin **3**. The glycoconjugated benzaldehyde **7** was obtained by amidation of the carboxybenzaldehyde using two equivalents of *O*-acetylated glucosamine and the coupling reagents DCC-BtOH in DMF-CH_2Cl_2. The deprotection of the aldehyde function (partial imine formation was observed) was performed with hydrochloric acid (HCl) 5 N and the product obtained after chromatography column with a yield of 87%.

The *trans*-biglucosylated porphyrin has been synthesized using an intermediate step that is to say a glucosylated dipyrromethane. This dipyrromethane is stable in the purified form

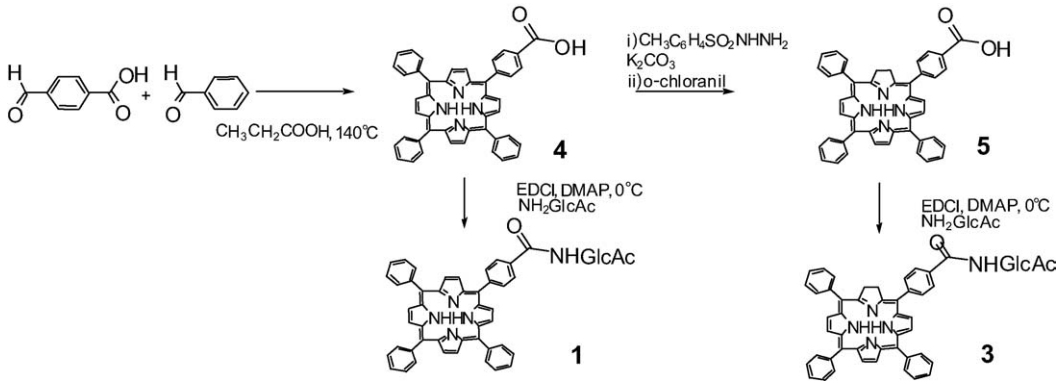

Scheme 1. Synthesis of 5-[4-(1,3,4,6-tetra-*O*-acetyl-2-amido-2-desoxy-β-D-glucopyranose phenyl)]-10,15,20-triphenyl porphyrin (**1**) and 5-[4-(1,3,4,6-tetra-*O*-acetyl-2-amido-2-desoxy-β-D-glucopyranose phenyl)]-10,15,20-triphenyl chlorin (**3**).

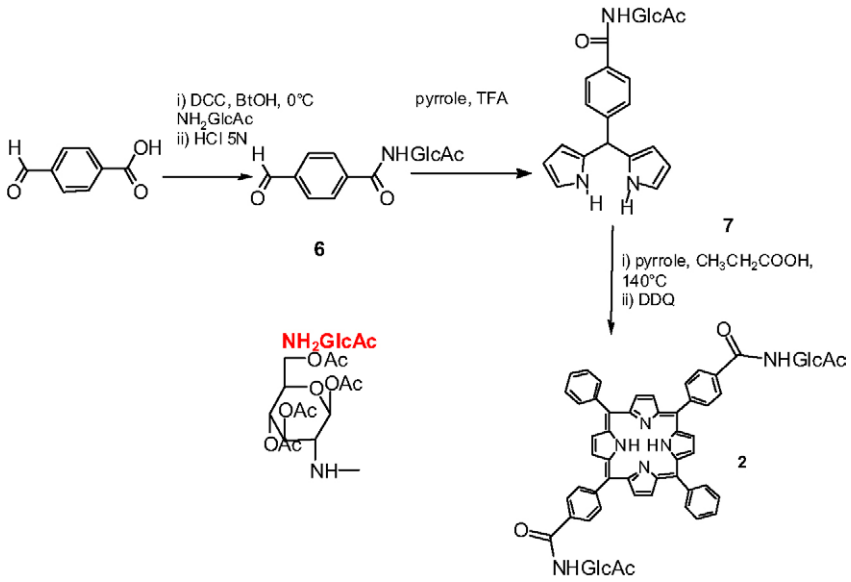

Scheme 2. Synthesis of 5,15-bis[4-(1,3,4,6-tetra-*O*-acetyl-2-amido-2-desoxy-β-D-glucopyranose phenyl)]-10,20-biphenyl porphyrin (**2**).

in absence of light and air and the reaction of the *meso*-substituted dipyrromethane with the benzaldehyde under the conditions of the two-step one flask porphyrin synthesis affords a direct route to *trans*-substituted *meso*-porphyrin [15]. The synthesis was carried out by condensation of the acetylglycoconjugate benzaldehyde with a large excess of pyrrole and a catalytic amount of trifluoroacetic acid (TFA). The yield is 85%. The dipyrromethane could be then condensed with the benzaldehyde to afford the *trans*-substituted porphyrin **2**.

The purification was done by chromatography and the pure product was obtained with 7% yield, which is acceptable for this kind of synthesis. The structures of the purified conjugates were corroborated by ^{1}H nuclear magnetic resonance spectroscopy (NMR), UV–Vis analysis and mass spectra (MALDI-TOFMS, data not shown).

We chose to study glucosamide conjugates of **4** in which the β-glucose is protected. Indeed, we previously demonstrated that when glucosylated fluorescent tracers had hydroxyl-protected sugar with acetyl groups, they did not cause toxicity in comparison with those linked with free hydroxyl sugars [16]. Moreover, Mikata et al. [17] reported the in vitro photocytotoxicity of four families of hydroxyl-protected and unprotected sugar-linked TPPs, in order to clarify the effect of amphiphilic character and carbohydrate recognition on photodynamic activity. The in vitro photocytotoxic results of tetracarbohydrated porphyrins indicated that the glucose moiety protected with acetyl groups specifically increased the incorporation of the drug into the cell [17].

2.1.2. Photophysical characteristics

The absorption spectra of photo-active compounds were typical of porphyrin derivatives with a Soret band of about 417 nm with high extinction coefficient (ε, Table 1) and four Q bands at ca. 515, 550, 590 and 650 nm (Fig. 1). The presence of amino glucosylated groups leads to a low decrease of extinction coefficients in the Soret band (Table 1). As expected, **3** displayed a high extinction coefficient value at 650 nm compared to porphyrins (Table 1).

The fluorescence quantum yield values were calculated by steady state comparative method using TPP as a reference [18]. The fluorescence quantum yield values were comparable (Table 1). Singlet oxygen formation quantum yields values were calculated by direct measurement of the infrared luminescence (1270 nm), using TPP as a reference. **3** displayed the highest $\Phi\ ^1O_2$ value (Table 1) and it was the only chlorin tested in this study. This result is in good agreement with Mikata et al. who demonstrated that the sugar-linked chlorins were more effective than TPP tetrasulfonic acid

Table 1
Molar extinction coefficients (ε), fluorescence emission maximum wavelength (λ_{max}), fluorescence (Φ_f) and singlet oxygen formation ($\Phi\ ^1O_2$) quantum yields, and triplet state lifetimes (τ)

Photosensitizer	λ_{max}	ε [a]	λ (nm)	ε	λ_{max}	Φ_f	$\Phi\ ^1O_2$	τ_1	τ_2
	Soret band		Q bands						
1	415	117	650	1.2	652/720	0.09	0.55	1.15 ± 0.03	35 ± 6
2	420	149	646	3.9	654/718	0.1	0.33	*n.d.*	*n.d.*
3	415	58	650	6.9	652/720	0.16	0.73	1.03 ± 0.03	70 ± 17
TPP	417	556	650	3.4	654/718	0.11	0.55	1.45 ± 0.08	66 ± 12

τ_1: Triplet state life time in aerated solution (μs).
τ_2: Triplet state life time in argon saturated solution (μs).
n.d.: Not determined.
[a] (10^3 l mol^{-1} cm^{-1}).

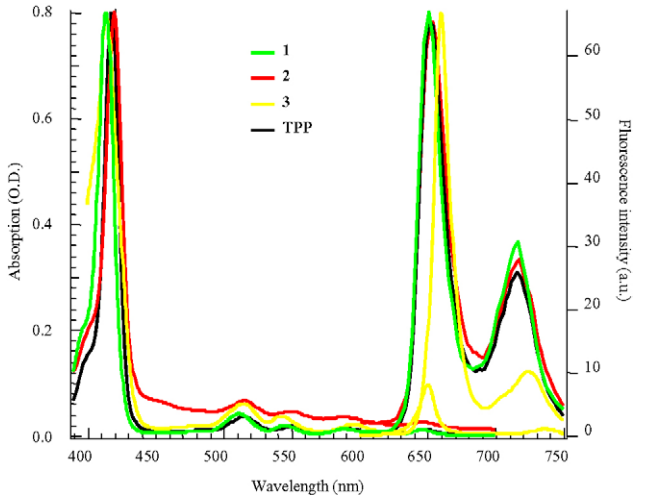

Fig. 1. Absorption and emission spectra of the glucosylated compounds and TPP in ethanol (normalized). For emission spectra, excitation wavelength was performed at 417 nm.

which is known as a photosensitizer that produce singlet oxygen efficiently [19]. Singlet oxygen formation quantum yields seem to be influenced by the number of glucosylated group, illustrating that the changes in the structure could influence the triplet quantum yield and/or the efficiency of energy transfer to molecular oxygen (Table 1). Oulmi et al. have found a linear dependence between the number of the aryl groups of the glucosylated porphyrins and the singlet oxygen formation [20]. In our case, only the number of sugars changes and the few compounds tested does not allow us to discuss any correlation. **1** and **3** triplet state lifetimes were measured by laser flash photolysis in the presence of aerated solution and in argon-saturated solutions. Typical triplet–triplet absorption spectrum is shown on Fig. 2. The triplet–singlet difference spectra show a maximum absorption in the blue spectral region at 450 nm. The first peak sometimes found in the porphyrin triplet–triplet absorption spectrum [21] located in the near-UV region (330–350 nm) can not be distinguished from the noise. In the presence of oxygen, the decays follow a first-order dependence (data not shown) and this is essentially the same under nitrogen. The triplet states of these compounds are efficiently quenched by oxygen (Table 1).

2.1.3. Chemical characteristics

The amphiphilicity of dyes is a characteristic, which may be decisive for photosensitizing activity since this parameter may influence their ability to cross membrane as well as their localization within the cell. High performance liquid chromatography (HPLC) analysis allows us to compare the hydrophobic characteristic between the different photo-active compounds. This was done by reverse phase liquid chromatography. The retention times for TPP, **2** and **1** were 35.60 ± 0.04, 26.3 ± 0.03 and 23.3 ± 0.05 min, respectively.

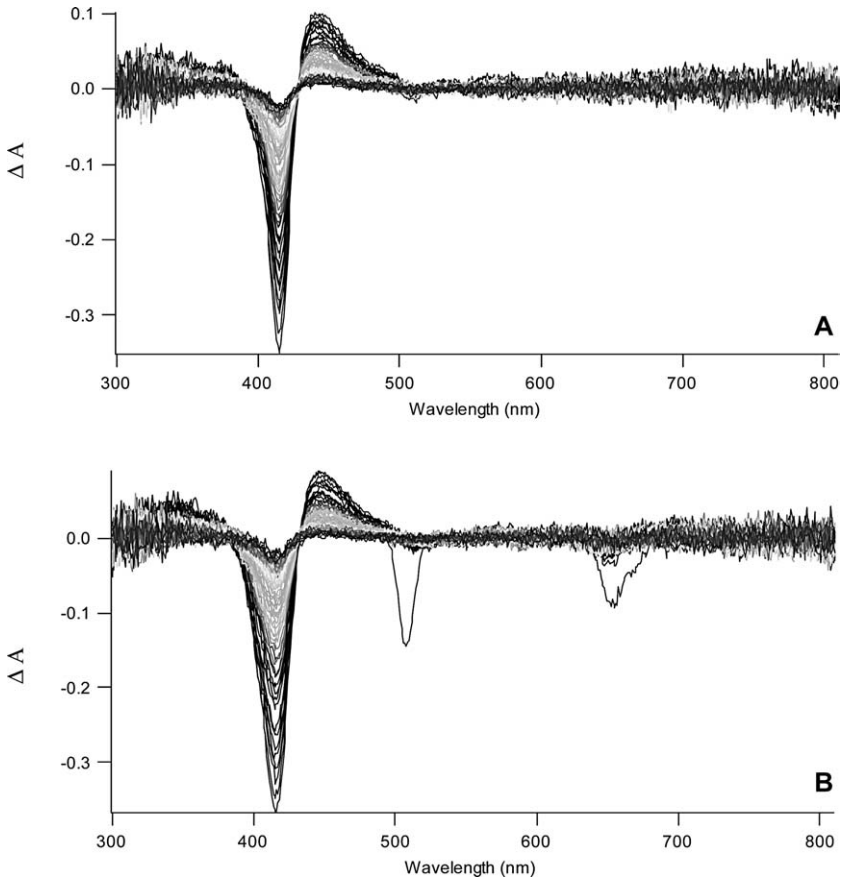

Fig. 2. Transient absorption spectrum (λ_{exc}, 515 nm and increment, 50 ns) (c) of **1** [A] and **3** [B] in DMSO with quenching constants (KQ), 98×10^4 and 111×10^6 l mol^{-1} s^{-1}, respectively.

Both isomers were found for **3**: 18.1 ± 0.02 and 18.9 ± 0.02 min. Actually, isomeric 2,3- and 7,8 mono-glucosylated chlorins were obtained as an inseparable mixture. These two isomers are different by the position of the reduced double bond in the macrocycle. TPP was the most hydrophobic compound and conversely, **3** was more hydrophilic than mono- and di-glucosylated porphyrins. The increase of acetylated D-glucosamine group number around the macrocycle confers a decrease of hydrophobic character to the compounds, confirmed by the values of retention times. Aggregation and hydrophobicity are conclusive factors, which can influence photosensitizer uptake [9]. For in vitro quantitative structure-activity relationship studies, it was noted that amphiphilic compounds exhibit greater photosensitizing ability than symmetrically hydrophobic or hydrophilic compounds [22]. This was most clearly demonstrated by studies showing that disulfonated phthalocyanines and TPPs with the two sulfonate groups adjacent to each other were more active than derivatives with two sulfonate groups on opposite sides of the chromophore [23].

2.2. Cellular uptake kinetics

The HT29 cellular uptake of TPP, **1**–**3**, as a function of incubation times, was examined for a non-cytotoxic photosensitizer concentration (10 μM, Fig. 3). During the first 3 h, the photosensitizers accumulated similarly in HT29 cells with no significant difference in the mean normalized fluorescence intensities of the cell suspension. From 15-h incubation, the accumulation of glucosylated photosensitizers was significantly higher ($P < 0.05$) than the cellular uptake of TPP (Fig. 3). The cellular uptake of **1** after a 24-h exposure was on average about 11.5-fold higher than the concentration of TPP and the accumulation of **2** and **3** compounds reached 5.0- and 6.4-fold more, respectively. The intracellular kinetic experiments of glucosylated compounds demonstrated that a steady state was reached at about 20 h. It may be noted that accumulation can be related to the dye retention time values, higher hydrophobicity (TPP) corresponding to lower uptake. For mono- or di-glucosylated compounds (**1** and **2**), it is not so clear as position of sugar substituent could also influence cellular uptake and photobiological activity. Improvement of cellular uptake for the glucosylated compounds was partly related to the increase of their hydrophilicity. Nevertheless, gross cellular uptake was not in itself the only determinant of PDT activity, but localization to a sensitive subcellular target may be important. In this current study, fluorescence microscopy was used to examine the subcellular localization patterns of glucosylated compounds.

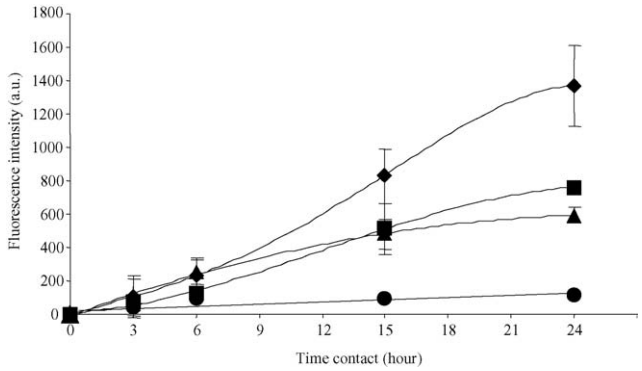

Fig. 3. Cellular uptake time course as determined from the cellular fluorescence of HT29 intensities with [lozenge] **1**, [triangle] **2**, [square] **3**, and [circle] TPP at 10 μM. Cellular fluorescence intensities were measured at 650 nm. For each experiment, the fluorescence intensity of each sample was normalized to cell concentration.
These data represent the mean values from three or four independent experiments. Error bars are standard deviations.

2.3. Antiproliferative assay

The 3-(4,5-dimethylthiazol-2-yl)-2,5-diphenyltetrazolium bromide (MTT) test was used to evaluate the cytotoxicity of TPP, **1**–**3** in the dark for concentrations varying from 0.5 to 30.0 μM (Fig. 4). Experiments, yielding surviving cell fractions higher than 85%, demonstrated that incubation of HT29 cells with the above TPP concentrations for 24 h, induced no cytotoxicity in the absence of light exposure. Fig. 4 demonstrates that 24-h incubation with mono-glucosylated compounds (**1** and **3**) induced no cytotoxicity for concentrations lower than 10 μM. However, **2** revealed more cytotoxic effects than mono-glucosylated compounds (Fig. 4).

2.4. Photocytotoxicity

The cells were incubated with the photo-active compounds at 10^{-6} M and irradiated by red light as we previously described [24], except that HT29 cells were exposed to the dye for 24 h at 37 °C. The intracellular uptake kinetics demonstrated that a steady state was reached at about 20-h exposure (Fig. 3). Because one aim of this work was to improve photosensitization to red light, which is a light wavelength able to enter deeply in living tissues, we compared the activity of glucosylated compounds and of TPP following red light irradiation (λ = 650 nm, fluence 4.54 mW cm^{-2}). The light

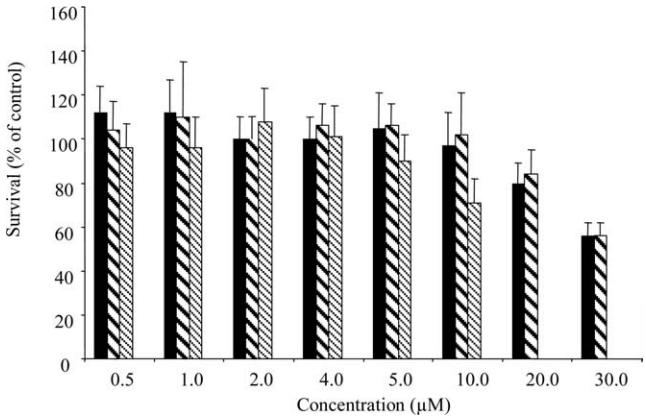

Fig. 4. Survival of HT29 cells treated with [black] **1**, [wide shading] **3**, [fine shading] **2** for 24-h incubation without irradiation. Concentration dependence of cytotoxicity for glucosylated compounds. Experiments were performed by MTT test. Data represent the mean values from three independent experiments. Error bars are standard deviations.

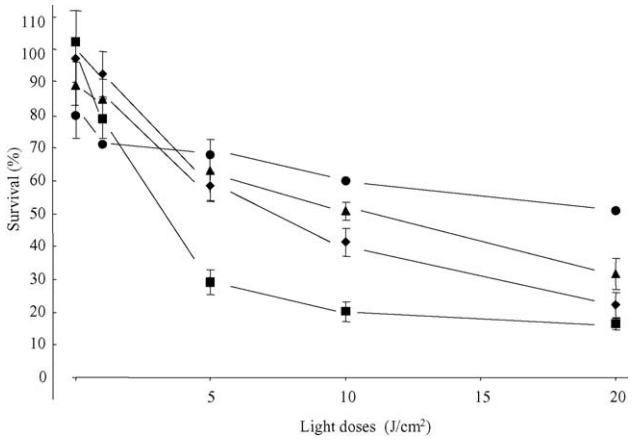

Fig. 5. Measurement of PDT sensitivity for [lozenge] **1**, [triangle] **2**, [square] **3**, and [circle] TPP in HT29 cells. Survival curves, obtained by MTT test, were assessed for cells exposed to increasing doses of light from 1.0 to 20.0 J cm^{-2} (for details see Section 4.6). Cells were incubated with photosensitizers at 10^{-6} M for 24 h before light treatment. Data represent the mean values from three independent experiments. Error bars are standard deviations.

doses yielding 50% growth inhibition ($L.D._{50}$) values of **3**, **1**, **2** and TPP were 4.4, 5.2, 11.1 and 30.2 J cm^{-2}, respectively. Thus, **3** and **1** were statistically significantly more efficient 6.9-fold and 5.8-fold, respectively, compared to TPP ($P < 0.05$). Fig. 5 shows that TPP control photosensitizer displayed a low photocytotoxicity in our experimental conditions. Conversely, survival measurements with the MTT test demonstrated that using glucosylated compounds, the photosensitivity was improved in comparison to TPP-mediated photosensitization (Fig. 5). The lowest uptake observed for TPP is consistent with the lowest photosensitivity ($L.D._{50}$ = 30.2 J cm^{-2}) and the most pronounced photodynamic activity measured for **3** ($L.D._{50}$ = 4.4 J cm^{-2}) is in relation with the improvement of cellular uptake (6.4-fold), the high $\Phi\ ^1O_2$ value (0.73) and the high extinction coefficient value at 650 nm compared to porphyrins.

The **2** symmetric glucosylated porphyrin exhibited a low photocytotoxicity compared to **1**. This observation confirms conclusions previously described. It was found that compounds bearing asymmetric mono-saccharide units are, in general, more phototoxic than symmetrical compounds [9].

2.5. Visualization of cellular uptake and subcellular localization

Cellular uptake of TPP and **1** (1 μM) was also compared using confocal fluorescence microscopy by incubating HT29 cells for 24 h (Fig. 6). The cells displayed a pattern of weak intracellular TPP fluorescence emission, indicative of extensive intracellular aggregation (Fig. 6D). Moreover, this fluorescence emission appeared more restricted to the cytoplasmic compartment with little or no detectable nuclear staining observed. With the same concentration employed with TPP, the cells exhibited an intense and diffuse intracellular **1** fluorescence (Fig. 6E). Comparable staining was observed with **3** (Fig. 6F). The diffuse cytoplasmic fluorescence observed for cells treated with glucosylated photosensitizers is consistent with previous results reported in literature [25]. Fig. 6 clearly shows the advantage of introduction of sugar moiety in membrane permeability of sugar-linked photosensitizer.

Confocal images of the double stained HT29 cells with **1** and $DiOC_6$ endoplasmic reticulum marker are presented in Fig. 7. The representative image of **1** is shown in red (Fig. 7B), the organelle-specific dye in green (Fig. 7A), and the overlapped image in yellow (Fig. 7C). Subcellular localization analysis with organelle probes in HT29 cells shows that **1** accumulated mainly inside the endoplasmic reticulum (Fig. 7C). Fluorescence topographic profiles of $DiOC_6$ and of **1** checked and proved this localization (Fig. 8). The mitochondrial image showed no overlap with the corresponding **1** image. Moreover, accumulation and the staining pattern of lysosomal probe Lucifer Yellow® and **1** were different, thus indicating that very little **1** accumulated inside lysosomes (data not shown). According to Laville et al., the tri-glucoconjugated chlorin could be partly internalized via an active receptor-mediated endocytosis mechanism and this higher phototoxicity has been related to a greater mitochondrial affinity [25]. In our case, mitochondrial-localizing mitotracker® and **1** fluorescence patterns were different, indicating a poor affinity of **1** for this organelle. There is strong evidence that photosensitizers with an acute localization in mitochondria promote the release of cytochrome c upon irradiation [26]. This loss of cytochrome c can be lethal to cells either because of the disruption of the mitochondrial respiratory chain with the eventual reduction of cellular ATP levels, or through caspase initiation with subsequent apoptotic cell death [27]. The impact of PDT on the endoplasmic reticulum has not very often been taken into account. Only a few studies have demonstrated the importance of photochemical damage to endoplasmic reticulum for the inactivation of tumor cells in culture [28–31]. The endoplasmic reticulum is mainly localized in the perinuclear area of the cytoplasm, and like Golgi apparatus they also interact together in the case of newly synthesized proteins. The endoplasmic reticulum is known to play a central role in the biosynthesis, segregation, and transport of proteins and lipids, as well as in the release of intracellular stores of calcium [32].

We can also add that using protected sugar motifs acts in favor of endoplasmic reticulum localization. Actually, we previously demonstrated that coumarins linked with free glucosamine presented an intracellular fluorescence distribution in the cytoplasmic compartment whereas those protected with acetylated glucosamine showed an accumulation inside the endoplasmic reticulum [16].

3. Conclusions

Our results show that glycoconjugation is obviously an interesting means to introduce such a balance between hydro-

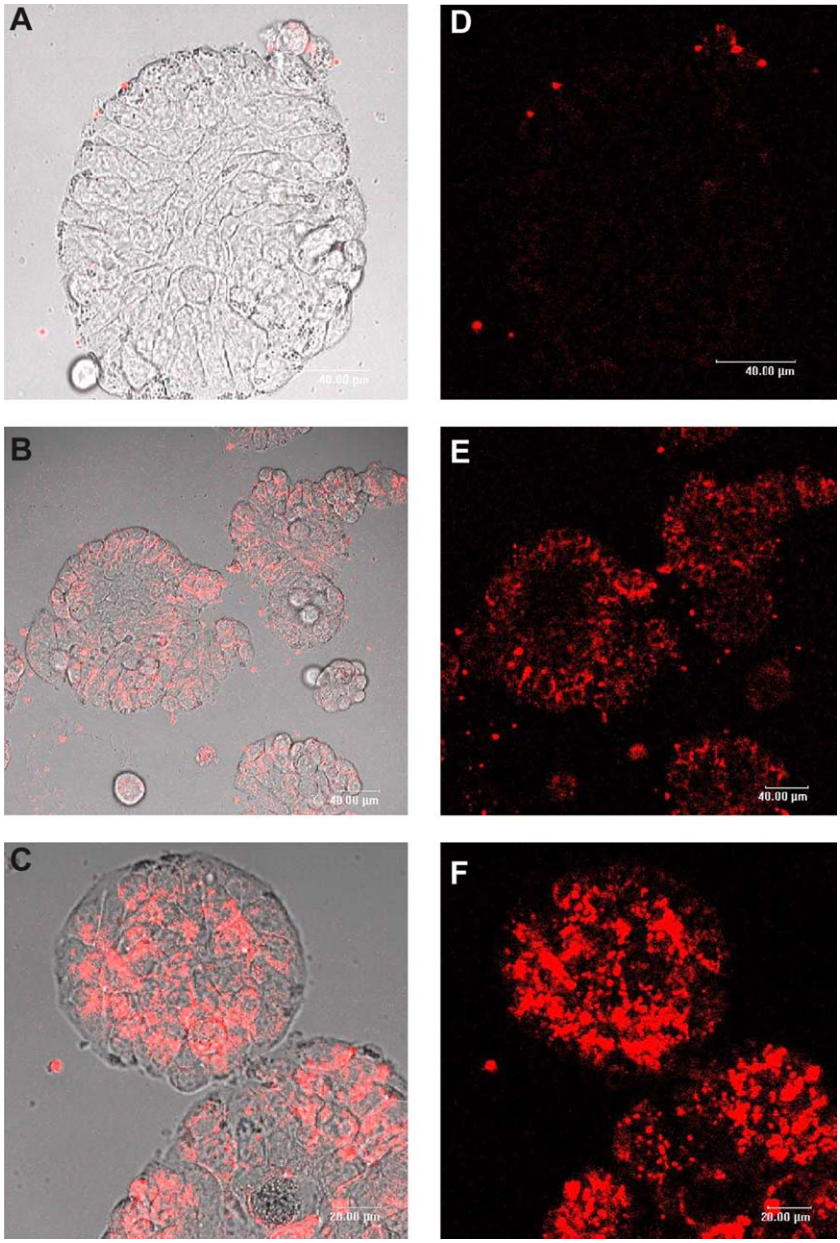

Fig. 6. Visualization of cellular uptake by confocal fluorescence microscopy for HT29 cells exposed for 24-h incubation to TPP (A, D); **1** (B, E) and **3** (C, F). Light transmitted (left column) and the corresponding fluorescence images (right column). Scale bars are indicated on images.

phylicity and hydrophobicity, previous observations suggesting the requirement of amphiphilicity for efficient photodynamic activity [33]. Thus, the improvement of cellular uptake achieved for glucosylated compounds, was partly related to the increase of hydrophylicity. The cellular uptake of **1** was on average about 11.5-fold higher than the concentration of TPP and the accumulation of **3** reached 6.4-fold more. The higher photodynamic efficiency has been related to this greater cellular uptake. Survival measurements using photocytotoxicity assay demonstrated that HT29 cells were significantly more sensitive to asymmetric mono-glucosylated photosensitizer-mediated PDT. Visualization of cellular uptake demonstrated that the cells displayed a pattern of weak intracellular TPP fluorescence emission, associated with an intense intracellular aggregation. Subcellular localization analysis with organelle probes showed that **1** accumulated mainly inside the endoplasmic reticulum. Thus, we have successfully synthesized new glucosylated porphyrins and chlorin, which could be considered as potential agents in cancer phototherapy.

4. Experimental

4.1. Synthesis

Chemicals and solvents were purchased from Aldrich (Saint Quentin Fallavier, France) and SdS (Peypin, France). Reactions were monitored by thin-layer chromatography (Kieselgel 60 F254, SdS). Chromatographic purification was performed with silical gel (200–400 mesh).

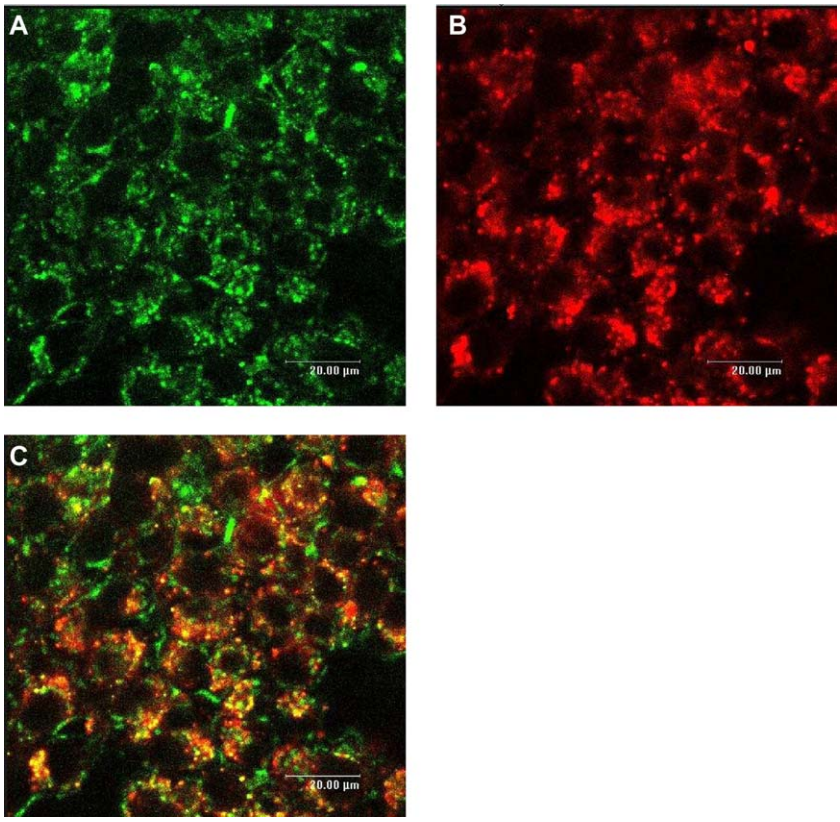

Fig. 7. Confocal fluorescence microscopy images of HT29 cells, double stained with **1** and an organelle probe. Dual staining confocal microscopy was performed for **1** emitting a red fluorescence signal (B). The cells were exposed to $DiOC_6$ (A) staining the endoplasmic reticulum (green fluorescence) and the overlapped image in yellow (C). The cells were exposed for 24-h incubation to **1** (1 µM), then exposed to $DiOC_6$ (C).
Scale bars are indicated on images.

NMR spectra were recorded on a Avance Brucker 300 MHz spectrometer. ^{1}H NMR spectra are reported in units of δ with tetramethylsilane (TMS) resonance at 0 ppm as a reference.

MALDI sample preparation: a saturated α-cyano-4-hydroxy-*trans*-cinnamic acid (CHCA) solution, in 50% acetonitrile, 0.1% of trifluoroacetic acid, and 1 µl of sample were spotted on the stainless steel MALDI targets. The molar ratio of analyte to matrix was 1:10^4. The solvent was evaporated prior to insertion in the source. Mass spectra were acquired over the range 0–3000 Da.

The porphyrins and chlorin and the general procedure of their synthesis are reported in Schemes 1 and 2.

5-(4-Carboxyphenyl)-10,15,20-triphenyl-21,23-porphyrin (**4**) was synthesized via condensation of benzaldehyde, 4-carboxybenzaldehyde and pyrrole under acid catalysis [34].

*4.1.1. Synthesis of 5-[4-(1,3,4,6-tetra-*O*-acetyl-2-amido-2-desoxy-β-D-glucopyranose phenyl)]-10,15,20-triphenyl porphyrin (**1**)*

To a solution of 2-amino-1,3,4,6,-tetra-*O*-acetyl-2-deoxy-β-D-glucose (0.147 mmol, 51 mg) and 5-(4-carboxyphenyl)-10,15,20-triphenyl-21,23-porphyrin (0.147 mmol, 100 mg) in CH_2Cl_2 was added 1.1 eq. of 1-(3-dimethylaminopropyl)-3-ethyl-carbodiimide (0.162 mmol, 31 mg) and catalytic amount of DMAP (0.015 mmol, 1.8 mg). The mixture was stirred for 3 h at 0 °C and 24 h at room temperature. The solution was then washed with 1 N HCl, $NaHCO_3$ saturated solution, distilled water and dried over magnesium sulfate ($MgSO_4$).

The compound was purified by SiO_2 chromatography using 3:97 EtOH/CH_2Cl_2. The yield is 65%.

Rf 0.52 (SiO_2, 4:96 EtOH/CH_2Cl_2), mp 184 °C, ^{1}H NMR ($CDCl_3$) δ: –2.70 (s, 2H, NH), 2.18 (s, 3H, CH_3), 2.23 (s, 3H, CH_3), 2.24 (s, 3H, CH_3), 2.32 (s, 3H, CH_3), 4.00 (m, 1H, Glc-H-5), 4.30, 4.42 (m, 2H, Glc-H-6, CH_2OAc), 4.80 (m, 1H, Glc-H-2), 5.41 (m, 2H, Glc-H-3, Glc-H-4), 6.01 (d, 1H, Glc-H-1, J = 8.7 Hz), 6.58 (s, 1H, CONH), 7.81 (m, 9H, Phenyl), 8.12 (2H, d, ArH, J = 8.2 Hz), 8.26 (2H, ArH), 8.40 (m, 2H, d, ArH, J = 8.2 Hz), 8.82, 8.91 (m, 8H, pyrrole-H), MS (MALDI-TOFMS) m/z: 988.35 Da.

*4.1.2. Synthesis of the 4-(1,3,4,6-tetra-*O*-acetyl-2-amido-2-desoxy-β-D-glucopyranose) benzaldehyde (**6**)*

A solution of 4-carboxybenzaldehyde (1 mmol, 0.150 g) in 10 ml CH_2Cl_2 was cooled to 0 °C under argon atmosphere. 1-hydroxybenzotriazole (BtOH) (1.2 mmol, 0.162 g) in 4 ml DMF and then DCC (1.2 mmol, 0.247 g) in 5 ml CH_2Cl_2 was added drop by drop. The solution was stirred for 2 h at room temperature. 2-Amino-1,3,4,6,-tetra-*O*-acetyl-2-deoxy-β-D-glucose (2 mmol, 0.694 g) in 5 ml was added to the mixture which was allowed to stir all night. The mixture was then filtered and the solvent was removed under reduced pressure. The

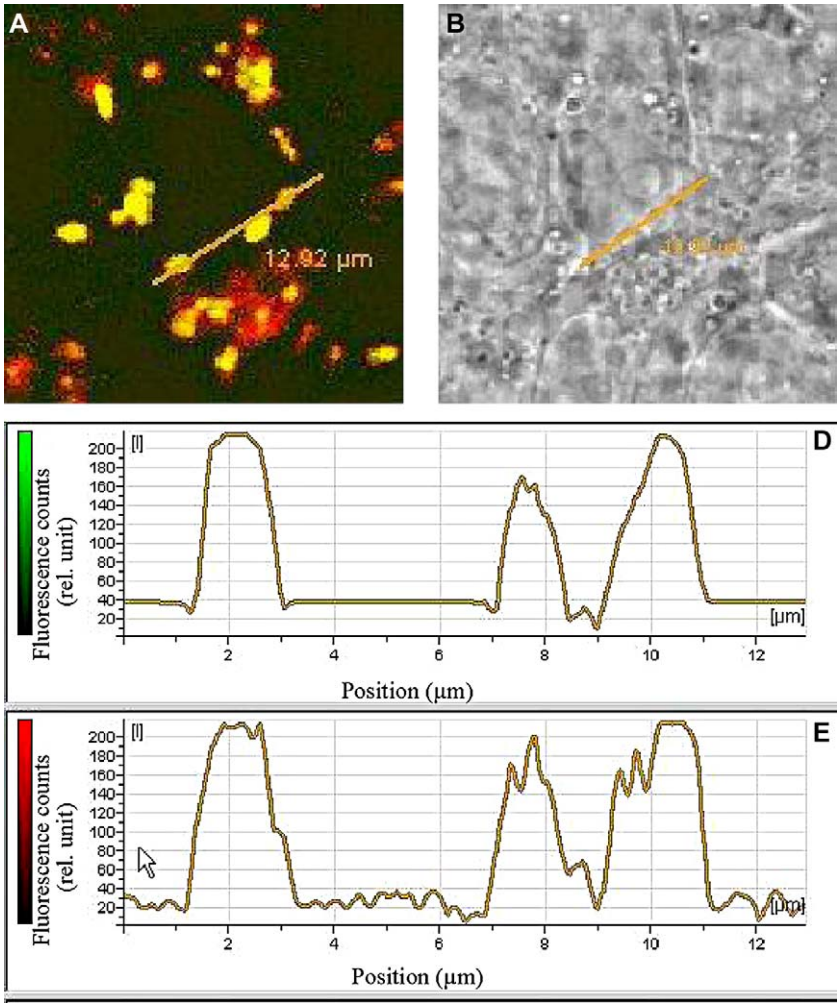

Fig. 8. Confocal fluorescence microscopy images of HT29 cells double stained with **1** and $DiOC_6$ (A) and the corresponding image obtained by transmission (B). Fluorescence topographic profiles of $DiOC_6$ (D) correspond to the endoplasmic reticulum (D) and **1** (E) corresponds to mono-glucosylated porphyrin.

deprotection of the aldehyde function (partial imine formation was observed) was realized with 3 ml HCl 5 N in 30 ml acetone. The mixture was stirred for 15 min and acetone was removed under reduced pressure. The product was dissolved in CH_2Cl_2, the organic phase was washed with HCl 1 N, water and dried ($MgSO_4$). The solvent was removed under reduced pressure. The product was obtained with 87% yield.

Rf 0.66 (SiO_2, 4:96 EtOH/CH_2Cl_2), m.p. 157 °C, ^{1}H NMR ($CDCl_3$) δ: 2.07 (s, 3H, CH_3), 2.12 (s, 3H, CH_3), 2.13 (s, 3H, CH_3), 2.21 (s, 3H, CH_3), 3.50 (1H, m, Glc-H-2), 3.86 (1H, m, Glc-H-5), 4.21, 4.30 (2H, dd, Glc-H-6), 5.28 (2H, m, Glc-H-3, Glc-H-4), 5.84 (1H, d, Glc-H-1, J = 8.8 Hz), 6.35 (1H, s, NHCO), 7.86, 7.97 (4H, d, Ar–H, J = 8.1 Hz), 10.1 (1H, s, CHO).

*4.1.3. Synthesis of meso-(4(1,3,4,6-tetra-*O*-acetyl-2-amido-2-desoxy-β-*D*-glucopyranose) phenyl dipyrromethane (**7**)*

A solution of the glycoconjugated benzaldehyde **6** (0.45 mmol, 200 mg) and pyrrole (18 mmol, 1.3 ml) was degassed by bubbling with argon for 10 min. Trifluoroacetic acid (0.045 mmol, 3.6 µl) was added. The solution was stirred for 15 min more at room temperature. The mixture was then diluted with CH_2Cl_2 (50 ml) and washed with 0.1 N aq. NaOH, water and dried with $MgSO_4$. The solvent was removed under reduced pressure and the unreacted pyrrole by vacuum distillation at room temperature. The white product is purified by chromatography on SiO_2, using 4:96 EtOH/CH_2Cl_2, the yield is 85%.

Rf 0.37 (SiO_2, 4:96 EtOH/CH_2Cl_2), m.p. 250 °C, ^{1}H NMR ($CDCl_3$) δ: 1.92 (s, 3H, CH_3), 1.99 (s, 3H, CH_3), 2.00 (s, 3H, CH_3), 2.04 (s, 3H, CH_3), 3.75 (m, 1H, Glc-H-5), 4.08, 4.23 (d, 2H, Glc-H-6 CH_2OAc), 4.46 (m, 1H, Glc-H-2), 5.16 (m, 2H, Glc-H-3, Glc-H-4), 5.44 (s, 1H, CH), 5.72 (d, 1H, Glc-H-1, J = 8.7 Hz), 5.81 (m, 2H, pyrrole), 6.06 (m, 2H, pyrrole), 6.10 (s, 1H, CONH), 6.64 (s, 2H, pyrrole), 7.22 (d, 2H, ArH, J = 8.1 Hz), 7.56 (d, 2H, ArH, J = 8.1 Hz), 7.89 (broad band, 2H, NH pyrrole), MS.

*4.1.4. Synthesis of 5,15-bis[4-(1,3,4,6-tetra-*O*-acetyl-2-amido-2-desoxy-β-*D*-glucopyranose pheny)]-10,20-biphenyl porphyrin (**2**)*

A solution of *meso*-(4-(1,3,4,6-tetra-*O*-acetyl-2-amido-2-desoxy-β-D-glucopyranose)) dipyrromethane (0.2 mmol, 119 mg) and benzaldehyde (0.2 mmol, 21 mg) in 20 ml

CH_2Cl_2 was purged with argon for 15 min, then trifluoroacetic acid (0.2 mmol, 15 μl) was added. The mixture was stirred for 2 h at room temperature then DDQ (0.4 mmol, 91 mg) was added. The mixture was stirred for 1 more h and the solvent was evaporated. The compound was purified by SiO_2 chromatography using 5:95 EtOH/CH_2Cl_2. The yield is 6%.

Rf 0.37 (SiO_2, 4:96 EtOH/CH_2Cl_2), m.p. 186 °C, ^{1}H NMR (CDCl3) δ: –2.76 (s, 2H, NH), 2.15 (s, 3H, CH_3), 2.20 (s, 3H, CH_3), 2.22 (s, 3H, CH_3), 2.28 (s, 3H, CH_3), 3.80 (m, 1H, Glc-H-5), 4.30, 4.41 (m, 2H, Glc-H-6, CH_2OAc), 4.78 (m, 1H, Glc-H-2), 5.41 (m, 2H, Glc-H-3, Glc-H-4), 6.01 (d, 1H, Glc-H-1, J = 8.7 Hz), 6.54 (s, 1H, CONH), 7.82 (m, 6H, 4 ArH), 8.12 (d, 4 ArH), 8.23 (d, 4 ArH), 8.32 (d, 4 ArH), 8.84, 8.90 (d, 8H, pyrrole-H, J = 4.6 Hz), MS (MALDI-TOFMS) *m/z*: 1361.45 Da.

*4.1.5. Synthesis of 5-(4-carboxyphenyl)-10,15,20-triphenyl-21,23-chlorin (**5**)*

C1COOH was synthesized as described by Whitlock et al. [14]: 5-(4-carboxyphenyl)-10,15,20-triphenyl-21,23-porphyrin (0.15 mmol, 100 mg), toluenesulfohydrazide (0.30 mmol, 81 mg) and potassium carbonate anhydrous (1.35 mmol, 186 mg) in 7 ml of dry pyridin were refluxed under argon. Toluenesulfohydrazide in 0.2 ml of pyridin were added twice at intervals of 2 h. After 6.5 h of reaction, the solution was poured in a mixture of toluene and water (2:1) and stirred for 1 h under reflux at 90 °C. Organic phase was washed with 3 N HCl, water, saturated bicarbonate sodium solution and dried over $MgSO_4$. Visible spectrum of the product shows a mixture of chlorin and bacteriochlorin.

To the solution in toluene was added portions of tetrachloro-1,2-benzoquinone (0.08 mmol, 20 mg) at room temperature to oxidize the bacteriochlorin. Then the organic phase was washed with a solution of sodium hydroxide (NaOH) (5%), concentrated phosphoric acid (68 wt.%) to remove the residual porphyrin, water and saturated sodium bicarbonate ($NaHCO_3$) solution. The resulting solution containing only the chlorin was evaporated and the solid recrystallized in toluene (yield 72%).

Rf 0.38 (SiO_2, 4:96 EtOH/CH_2Cl_2), m.p. 94 °C, ^{1}H NMR (DMSO-d_6) δ: –1.59, –1.51 (s, 2H, NH), 4.13 (m, 4H, CH_2 chlorine), 7.46–8.30 (m, 6H pyrrole-H, 19 H phenyl). MS (MALDI-TOFMS) *m/z*: 656. 07 Da.

*4.1.6. 5-[4-(1,3,4,6-tetra-*O*-acetyl-2-amido-2-desoxy-β-*D*-glucopyranose pheny)]-10,15,20-triphenyl chlorin (**3**)*

A sample of **5** was treated identically as for **4**, affording a purple compound with 62% yield. Isomeric 2,3- and 7,8 mono-glucosylated chlorins showed two NH signals of almost equal intensity at –1.50 and –1.41 ppm, indicating a 1:1 mixture. They were obtained as an inseparable mixture.

Rf 0.62 (SiO_2, 4:96 EtOH/CH_2Cl_2), m.p. 200 °C, ^{1}H NMR ($CDCl_3$) δ: –1.50(s), –1.41(s) (2H, NH), 2.10–2.23 (m, 12H, 4 CH_3), 3.93 (m, 1H, Glc-H-5), 4.17 (m, 2H, CH_2 chlorine), 4.34, 4.38 (2H, Glc-H-6, CH_2OAc), 4.70 (m, 1H, Glc-H-2), 5.35 (m, 2H, Glc-H-3, Glc-H-4), 5.94 (m, 1H, Glc-H-1), 6.46 (m, 1H, CONH), 7.65–8.86 (m, 19H Phenyl, 6H pyrrole-H), MS (MALDI-TOFMS) *m/z*: 990.37 Da.

4.2. Absorption and fluorescence

Absorption spectra were recorded on a Perkin–Elmer (Lambda 2, Courtabœuf, France) UV–vis spectrophotometer.

Fluorescence spectra were recorded on a SPEX Fluorolog-2 spectrofluorimeter 1680 (Jobin Yvon, Longjumeau, France) equipped with a thermostated cell compartment (25 °C), using a 450 W Xenon lamp. Fluorescence quantum yields (Φ_f) were determined using a TPP solution as fluorescence standard (Φ_f = 0.11, in toluene, taking into account solvent refractive index and absorption efficiencies).

4.3. Determination of singlet oxygen quantum yield ($\Phi\ ^1O_2$)

Excitation occurred with a Xe-arc, the light was separated in a SPEX 1680, 0.22 μm double monochromator. The detection at 1270 nm was done through a PTI S/N 1565 monochromator, and the emission was monitored by a liquid nitrogen-cooled Ge-detector model (EO-817L, North Coast Scientific Co). The absorbance of the reference solution (TPP in $CHCl_3$ $\Phi\Delta$ = 0.55) [35] and the sample solution (at 515 nm) were set equal (between 0.2 and 0.5) by dilution.

4.4. Determination of triplet state lifetime τ

Laser flash photolysis was carried out at 295 K by using a Coherent Infinity YAG laser equipped with an optical parametric oscillator (OPO). The pulse duration and energy were 5 ns and 4 mJ, respectively. The illuminated surface area was 0.1 cm^2. Light from an EG and G FX504 low-pressure Xenon flash lamp passing through the sample under 90° with respect to the laser beam was used to probe the changes of the absorption spectra. The probe light was imaged using an Acton Research Spectra pro 150 spectrograph onto a Princeton Instruments ICCD-576-G/RB-EM gated intensified CCD camera (gate width 5 ns). The compounds were irradiated at 515 nm, in the Q_{IV} band, because of the gap in the spectral range of excitation of the Coherent Infinity YAG laser in the Soret band.

4.5. HPLC conditions

An Alltech Appollo C18, 5 μm column (250 × 4.6 mm internal diameter (I.D.), Alltech, Lokeren, Belgium) was used. Fluorescence detection was optimized with excitation and emission wavelengths of 414 and 650 nm, respectively.

Gradient elution conditions were adopted. The eluting solvent was methanol (MeOH)/H_2O (75:25, v/v) for 15 min, followed by 100% methanol for the last 25 min. Room temperature and a flow-rate of 1.0 ml min^{-1} were maintained throughout the analysis. A volume of 20 μl of the samples in

methanol was injected into the column. The internal standard stock solution of rhodamine 1 mg ml^{-1} was also prepared in methanol.

4.6. General procedure for in vitro experiments

4.6.1. Cell culture conditions

Human colorectal adenocarcinoma cells (HT29) were grown in 75 cm^2 plastic tissue culture flasks in RPMI 1640 medium supplemented with 9% heat inactivated fetal calf serum, penicillin (100 i.u. ml^{-1}), streptomycin (100 μg ml^{-1}) in an atmosphere of 37 °C and 5% CO_2 atmosphere. Cells were subcultured by dispersal with 0.25% trypsin and seeded 5×10^4 cells per ml.

4.6.2. Photosensitizers uptake

Cells (1.10^4 cells per ml) were inoculated in 25 cm^2 plastic tissue culture flasks and incubated for 72 h for proper attachment to the substratum. The HT29 cells were then exposed to photosensitizers (TPP, **1**, **3** and **2** at 10^{-5} M) in RPMI supplemented with 9% of bovine serum albumin (BSA) from 3 to 24 h. All stock solutions were prepared by dissolving 10^{-3} mol l^{-1} photosensitizer in DMSO and after diluted in RPMI in order to achieve dye concentrations mentioned. No cytotoxic effect of DMSO was checked. After incubation with the photosensitizers, the cells were washed twice in phosphate buffered saline (PBS), harvested by enzymatic desegregation [trypsin–ethylene diamine tetra acetic acid (EDTA)]. After, the cells were washed in ice-cold PBS using centrifugation ($200 \times g$) and the fluorescence from the drug-loaded cells was measured in 3.0 ml ethanol (EtOH) solution [36]. The fluorescence intensity of each sample was normalized to cell concentration, to molar extinction coefficient values at 417 nm and to fluorescence quantum yield assessed for each compound, respectively). Spectra were collected for wavelengths ranging from 600 to 750 nm (the band pass of both excitation and emission slits were 2.5 nm, in the case of drug-loaded cells 2.5 and 5.0 nm, respectively; the excitation wavelength was 417 nm; photomultiplier voltage was 770 V.

For all measurements, front surface accessories (Perkin–Elmer L225 9051) have been used, providing small angle (45°) front surface excitation geometry. All absorption spectra were recorded with a Perkin–Elmer Lambda Bio spectrophotometer, using a 10 mm quartz cuvette.

4.6.3. Cytotoxicity assays

Cell survival was measured using 3-(4,5-dimethylthiazol-2-yl)-2,5-diphenyltetrazolium (MTT) assay. Before performing growth inhibition assays, we examined the linearity of the MTT assay with increasing number of HT29 cells plated between 10^3 and 5.10^6 cells per ml and found quite satisfactory results ($r > 0.995$). Briefly, cells were seeded at the initial density of 1.10^4 cells per ml in 96-well microtitration plates. Forty-eight hours after plating, cells were exposed for 24 h to photosensitizers (TPP, **1**–**3**) for concentrations varying from 0.5 to 30 μM. After 24-h incubation at 37 °C, the medium was removed, cells were washed three times with cold PBS and fresh RPMI was added. Each concentration was tested in sextuplicate. As previously described [24] cell survival was measured 24 h after by MTT test; 50 μl of 0.5% MTT solution was then added in each well and incubated for 3 h at 37 °C to allow MTT metabolism. The formazan crystals were dissolved by adding 50 μl per well of 25% sodium dodecylsulfate solution and vigorous pipetting was performed. Absorbance was measured at 540 nm using a Multiskan MCC/340 plate reader (Labsystem, Cergy-Pontoise, France). Results were expressed as relative absorbance to untreated controls. Absorbance values for wells containing medium alone were subtracted from the results of test wells.

4.6.4. Photocytotoxicity assay

Cell survival was measured 24 h after photosensitization using MTT assay. HT29 cells were seeded at the initial density of 1.10^4 cells per ml in 96-well microtitration plates. Forty-eight hours after plating, cells were exposed to photoactive compounds at 10^{-6} M. After 24-h incubation at 37 °C, the medium was removed and cells were then washed three times with cold PBS and fresh RPMI was added before cell irradiation. Results are given as the percentage of the result obtained with the control cultures exposed to photosensitizer alone. Light doses, yielding 50% growth inhibition ($L.D._{50}$), were calculated using medium effect algorithm [37], and expressed as mean values of three independent experiments performed during different weeks. We used one plate for each dose of light from 1.0 to 20.0 J cm^{-2}. In order to perform the experiments exactly in the same conditions for the four photosensitizers (TPP, **1**–**3**), we divided each plate into four parts corresponding to each compound. The dark toxicity of photosensitizers was assessed separately following a similar procedure.

Irradiation was carried out at 650 nm, using a dye laser (Spectra Physics 375B) pumped with an Argon laser (Spectra Physics 2020, Les Ulis, France). The output power was 700 mW. The light spot was 14 cm in diameter, providing the fluence of 4.54 mW cm^{-2}. During irradiation, the temperature never exceeded 24 ± 2 °C. This temperature did not influence cell viability.

4.6.5. Treatment of cells prior to microspectrofluorimetry and confocal laser scanning microscopy

Dual staining confocal microscopy experiments were performed for **1**. Cells were plated at 10^3 cells per well in Labtek-II® 4-chambered coverslips (Dutscher, Brumath, France). After 48-h attachment at 37 °C, the cells were then incubated with **1** (10 μM) and specific organelle markers, according to the following protocol. Before observation, cells were then washed three times with RPMI medium and imaged using confocal laser scanning microscopy.

The organelles staining was investigated using the procedure adapted from the experimental protocol previously reported [38]. Endoplasmic reticulum was stained by incubating cells for 30 s at room temperature with 0.25 μg ml^{-1}

3,3-dihexyloxacarbocyanine iodide ($DiOC_6$). $DiOC_6$ was purchased from Molecular Probes, Leiden, The Netherlands. Mitochondria were identified after staining the cells for 30 s at 37 °C with 0.25 μmol l^{-1} Mitotracker Green® (Molecular Probes). For lysosomes identification, HT29 cells were incubated with **1** for 24 h, and overnight with 1 μg ml^{-1} Lucifer yellow, LY® (Sigma-Aldrich, France). The cells were then washed 3 times in a dye free media before imaging in RPMI.

The cells double stained with **1** and organelle probes were examined with a confocal laser scanning microscope (Leica TCS SP2-AOBS, Germany) equipped with an X63, numerical aperture 1.3 oil immersion objective (Leica). A pinhole of 60.85 μm was used and each image recorded contained 512 × 512 pixels. An argon laser was used as excitation light at 458 nm for all organelle probes and a helium/neon laser at 633 nm for **1**. Fluorescence of the organelles probes was detected on channel 1 with a 505–545 nm band pass emission filter. Channel 2 was used to detect the red fluorescence of **1** with 640–660 nm band pass emission filter. The fluorescence images were displayed in green and red "false" color output and electronically combined to visualize dual localization in yellow. Controls (cells stained only with **1** or organelle probes) were conducted in parallel to optimize the staining protocol and the detecting parameters of confocal laser scanning microscopy.

4.7. Statistical analysis

Mann and Whitney *U*-test was used to test for the significant level between independent variables. The level of significance was set to $P < 0.05$.

References

[1] J.G. Levy, M. Obochi, Photochem. Photobiol. 64 (1996) 737–739.
[2] T.J. Dougherty, Photochem. Photobiol. 45 (1987) 879–889.
[3] G. Poste, G.L. Nicolson, Biomembranes 11 (1983) 341–364.
[4] I. Rosenthal, Photochem. Photobiol. 53 (1991) 859–870.
[5] U. Isele, K. Schieweck, R. Kessler, P. van Hoogevest, H.G. Capraro, J. Pharm. Sci. 84 (1995) 166–173.
[6] I.J. MacDonald, T. Dougherty, J. Porphyrins and Phthalocyanines 5 (2001) 105–129.
[7] J.G. Moser, F.P. Montforts, D. Kusch, A. Vervoorts, D. Kirsch, M. Berghahn, N. Akgün, A. Rueck, S. Andrees, B. Wagner, Proc. SPIE, Int. Soc. Opt. Eng. 2924 (1996) 22–30.
[8] G. Zheng, A. Graham, M. Shibata, J. Missert, A.R. Oseroff, T.J. Dougherty, R.K. Pandey, J. Org. Chem. 66 (2001) 8709–8716.
[9] M. Momenteau, P. Maillard, M.A. de Bélinay, D. Carrez, A. Croisy, J. Biomed. Opt. 4 (1999) 298–318.
[10] M. Zhang, Z. Zhang, D. Blessington, H. Li, T.M. Busch, V. Madrak, J. Miles, B. Chance, J.D. Glickson, G. Zheng, Bioconjug. Chem. 14 (2003) 709–714.
[11] in: J. Defaye, J. Gelas (Eds.), Studies in Natural Products Chemistry, Elsevier, Amsterdam, 1991.
[12] M. Bergmann, L. Zervas, Ber. 65B (1932) 1201–1205.
[13] R.G. Little, J.Z. Anton, P.A. Loach, J. Heterocyclic Chem. 12 (1975) 343–349.
[14] H.W. Whitlock, R. Hanauer, M.Y. Oester, B.K. Bower, J. Am. Chem. Soc. 91 (1969) 7485–7489.
[15] C.H. Lee, J.S. Lindsey, Tetrahedron 50 (1994) 11427–11440.
[16] C. Geoffroy, M.C. Carré, F. Baros, S. Muller, D. Dumas, J.F. Stoltz, P. Van Hoppen, F.C. De Schryver, M.L. Viriot, in: Proceedings of the Third Conference on Fluorescence Microscopy and Fluorescent Probes, 1999, pp. 137–143.
[17] Y. Mikata, Y. Onchi, K. Tabata, S.I. Ogura, I. Okura, H. Ono, S. Yano, Tetrahedron Lett. 39 (1998) 4505–4508.
[18] J.N. Demas, G.A. Crosby, J. Phys. Chem. 75 (1971) 991–1024.
[19] Y. Mikata, Y. Onchi, K. Shibata, T. Kakuchi, H. Ono, S.I. Ogura, I. Okura, S. Yano, Bioorg. Med. Chem. Lett. 8 (1998) 3543–3548.
[20] D. Oulmi, P. Maillard, C. Vever-Bizet, M. Momenteau, D. Brault, Photochem. Photobiol. 67 (1998) 511–518.
[21] E. Reddi, G. Jori, M.A.J. Rodgers, J.D. Spikes, Photochem. Photobiol. 38 (1983) 639–645.
[22] R. Boyle, D. Dolphin, Photochem. Photobiol. 64 (1996) 469–485.
[23] D. Kessel, P. Thompson, K. Saatio, D. Nantwi, Photochem. Photobiol. 45 (1987) 787–790.
[24] M. Barberi-Heyob, P.O. Vedrine, J.L. Merlin, R. Millon, J. Abecassis, M.F. Poupon, F. Guillemin, Int. J. Oncol. 24 (2004) 951–958.
[25] I. Laville, T. Figueiredo, B. Loock, S. Pigaglio, P. Maillard, D.S. Grierson, D. Carrez, A. Croisy, J. Blais, Bioorg. Med. Chem. 11 (2003) 1643–1652.
[26] L.Y. Xue, S.M. Chiu, N.L. Oleinick, Exp. Cell Res. 263 (2001) 145–155.
[27] C.M. Yow, J.Y. Chen, N.K. Mak, N.H. Cheung, A.W. Leung, Cancer Lett. 157 (2000) 123–113.
[28] P. Morlière, J.C. Mazière, R. Santus, C.D. Smith, M.R. Prinsep, C.C. Stobbe, M.C. Fenning, J.L. Golberg, J.D. Chapman, Cancer Res. 58 (1998) 3571–3578.
[29] J.Y. Matroule, G. Bonizzi, P. Morlière, N. Paillous, R. Santus, V. Bours, J. Piette, J. Biol. Chem. 274 (1999) 2988–3000.
[30] C. Fabris, G. Valduga, G. Miotto, L. Borsetto, G. Jori, S. Garbisa, E. Reddi, Cancer Res. 61 (2001) 7495–7500.
[31] M.H. Teiten, L. Bezdetnaya, P. Morlière, R. Santus, F. Guillemin, Br. J. Cancer 88 (2003) 146–152.
[32] M. Terasaki, J. Song, J.R. Wong, M.J. Weiss, L.B. Chen, Cell 38 (1984) 101–108.
[33] A.S. Sobolev, D.A. Jans, A.A. Rosenkranz, Prog. Biophys. Mol. Biol. 73 (2000) 51–90.
[34] C.B. Hansen, G.J. Hoogers, W.J. Drenth, J. Mol. Catal. 79 (1993) 153–163.
[35] R. Schmidt, E. Afshari, J. Phys. Chem. 94 (1990) 4377–4378.
[36] C. Frochot, B. Di Stasio, M. Barberi-Heyob, M.C. Carré, J.M. Zwier, F. Guillemin, M.L. Viriot, Oftalmologia 56 (2003) 62–66.
[37] T.C. Chou, P. Talalay, in: K.R. Harrap, T.A. Connors (Eds.), New Avenues in Development Cancer Chemotherapy, Academic Press, New York, 1987, pp. 37–64.
[38] J.L. Merlin, H. Gautier, M. Barberi-Heyob, M.H. Teiten, F. Guillemin, Int. J. Oncol. 22 (2003) 733–739.